

Periodic Q-mode modulation in PSR J1825–0935 (PSR B1822–09)

W. M. Yan,^{1,2*} R. N. Manchester,³ N. Wang,^{1,2,4} J. P. Yuan^{1,2,4}
Z. G. Wen^{1,2} and K. J. Lee^{5,6}

¹*Xinjiang Astronomical Observatory, CAS, 150 Science 1-Street, Urumqi, Xinjiang, 830011, China*

²*Key Laboratory of Radio Astronomy, Chinese Academy of Sciences, Nanjing 210008, China*

³*CSIRO Astronomy and Space Science, Australia Telescope National Facility, PO Box 76, Epping, NSW 1710, Australia*

⁴*Xinjiang Key Laboratory of Radio Astrophysics, 150 Science 1-Street, Urumqi, Xinjiang, 830011, China*

⁵*Kavli Institute for Astronomy and Astrophysics, Peking University, Beijing 100871, China*

⁶*National Astronomical Observatories, Chinese Academy of Sciences, Beijing 100012, China*

Accepted XXX. Received YYY; in original form ZZZ

ABSTRACT

PSR J1825–0935 (PSR B1822–09) switches between radio-quiet (Q-mode) and radio-bright (B-mode) modes. The Q-mode is known to have a periodic fluctuation that modulates both the interpulse and the main pulse with the same period. Earlier investigators argued that the periodic Q-mode modulation is associated with drifting subpulses. We report on single-pulse observations of PSR J1825–0935 that were made using the Parkes 64-m radio telescope with a central frequency of 1369 MHz. The high-sensitivity observations revealed that the periodic Q-mode modulation is in fact a periodic longitude-stationary intensity modulation occurring in the interpulse and the main pulse. The fluctuation spectral analysis showed that the modulation period is about $43P_1$, where P_1 is the rotation period of the pulsar. Furthermore, we confirm that the modulation patterns in the interpulse and the main pulse are phase-locked. Specifically, the intensities of the interpulse and the immediately following main pulse are more highly correlated than for the main pulse and interpulse at any other lag. Polarization properties of the strong and weak Q-mode states are different, even for the trailing part of the main pulse which does not show the periodic intensity modulation.

Key words: stars: neutron – pulsars: general – pulsars: individual (PSR J1825–0935)

1 INTRODUCTION

PSR J1825–0935 (PSR B1822–09) is a well-known young pulsar which shows interpulse emission. As is shown in Figure 1, the mean pulse profile of PSR J1825–0935 consists of three main components: a strong and sharp main pulse (MP), a precursor (PC) preceding the MP by about 14.5° of pulse phase, and a relatively weak interpulse (IP) leading the PC by about 159° . This pulsar has attracted the attention of many investigators over the years because it exhibits three interesting features simultaneously: mode changing, IP-PC anticorrelation and periodic subpulse modulation.

PSR J1825–0935 is known to switch between two stable emission states at radio frequencies (Fowler et al. 1981; Morris et al. 1981; Gil et al. 1994). The PC drops to extremely low intensity in the Q-mode, while in the B-mode, it becomes relatively strong. Fowler & Wright (1982) reported

that the mode changing occurs approximately every 5 min. With a single 8-h GMRT observation, Latham et al. (2012) found that the average time between mode changes is about 7.6 min. From longer multifrequency observations made by three different radio telescopes (WSRT, GMRT and Lovell), Hermsen et al. (2017) found an average of one mode change every 3.5 min, but they did not find evidence for simultaneous X-ray and radio mode changing. PSR J1825–0935 also shows a correlation between the pulse shape and spin-down rate. Lyne et al. (2010) reported that pulse-shape changes between the Q-mode and the B-mode are highly correlated with the spin-down rate changes in PSR J1825–0935.

The most remarkable feature of PSR J1825–0935 is the peculiar and significant anticorrelation between the intensity of the IP and the PC. Observations revealed that the IP is visible when the PC is weak or absent (i.e., in the Q-mode); on the other hand, the IP becomes very weak or undetectable when the PC is present (i.e., in the B-mode) (Fowler & Wright 1982; Gil et al. 1994). Such an

* E-mail: yanwm@xao.ac.cn (WMY)

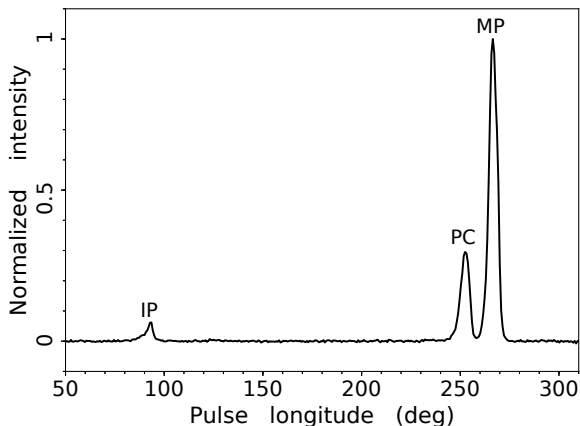


Figure 1. The integrated pulse profile of PSR J1825–0935 showing the three main components: interpulse (IP), precursor (PC) and main pulse (MP).

anticorrelation is naturally expected in models where the PC and the IP are generated at the same magnetic pole. Dyks et al. (2005) proposed that the IP and the PC originate from the same emission region and that the PC emission intermittently reverses its direction to form the IP. Although it is much harder to understand the IP-PC correlation in two-pole models, on the basis of the separation between the IP and the MP and/or polarization properties of this pulsar, many investigators argued that PSR J1825–0935 is an almost orthogonal rotator and that the IP and the PC are emitted from two opposite magnetic poles (Backus et al. 2010; Maciesiak et al. 2011; Latham et al. 2012; Hermsen et al. 2017).

Another curious property of PSR J1825–0935 is the periodic modulation in the Q-mode. Fluctuation-spectral analyses show that, in the Q-mode, the IP and the MP are modulated at the same period and their fluctuations are highly correlated (Backus et al. 2010; Latham et al. 2012). Latham et al. (2012) associated the periodic Q-mode modulation with subpulse drifting. However, no organized drifting pattern has been detected (Hermsen et al. 2017).

With high-sensitivity single-pulse observations, this paper aims to explore previously unknown properties of the periodic Q-mode modulation in PSR J1825–0935. Details of the observations and data processing are given in Section 2. In Section 3 we present details of the observed periodic intensity modulations. The implications of the results are discussed in Section 4.

2 OBSERVATIONS

The observational data analyzed in this paper were downloaded from the Parkes Pulsar Data Archive which is publicly available online¹ (Hobbs et al. 2011). The single-pulse observations were made using the Parkes 64-m radio telescope at six epochs with the center beam of the 20 cm Multibeam receiver (Staveley-Smith et al. 1996) and the Parkes digital filterbank systems PDFB3 and PDFB4. See

Manchester et al. (2013) for further details of the receiver and backend systems. For the observations reported here, the total bandwidth was 256 MHz centred at 1369 MHz with 512 channels across the band. The observing dates were 2013 March 25, June 23, 2014 February 20, April 19, July 28 and August 20. For each observation, the duration was 8 min and the sampling interval was 256 μ s.

The data were first reduced using the DSPSR package (van Straten & Bailes 2011) to de-disperse and produce single-pulse integrations which were recorded using the PSRFITS data format (Hotan et al. 2004) with 1024 phase bins per rotation period. The pulsar’s rotational ephemeris was taken from the ATNF Pulsar Catalogue V1.59² (Manchester et al. 2005). Strong narrow-band radio-frequency interference (RFI) in the archive files was removed in affected frequency channels. Broad-band impulsive RFI was also removed in affected time sub-integrations. Following Manchester et al. (2001), the single-pulse integrations were then corrected for an effective high-pass filter in the search-mode quantization algorithm. The corrected single-pulse integrations were processed using the PSRCHIVE software package (van Straten & Bailes 2011). The analysis of fluctuation spectra was carried out with the PSRSALSA package (Weltevrede 2016) which is freely available online³. Following Yan et al. (2011), the flux density, polarization and pcm calibration were carried out for one observation for later polarization analysis. The rotation measure (RM) value was obtained from Johnston & Kerr (2018). Polarization parameters are in accordance with the astronomical conventions described by van Straten et al. (2010).

3 RESULTS

The periodic fluctuation in the Q-mode of PSR J1825–0935, in which the IP and the MP are modulated at the same period, is well known from earlier studies. To see this feature more clearly, we plotted the pulse stack of the 2014 August 20 observation, which is a pure Q-mode observation, in Figure 2. The left and right panels show the single pulses of respectively the IP and MP for the same rotation of the pulsar, where the IP is assumed to precede the MP. The pulse energy variations with time of the IP and the leading region of the MP for the same observation are presented in Figure 3. The pulse phase windows for calculating the pulse energy were determined by eye (see Figure 2). Figure 2 gives the impression that the periodic modulation could be periodic nulling in the IP and the leading component of the MP. However, Figure 3 shows that the periodic modulation differs from pulse nulling in two key aspects. Firstly, it is generally believed that the transitions from bursts to nulls and the transitions from nulls to bursts are abrupt (e.g., Wang et al. 2007) rather than gradual as in Figure 3. Secondly, the pulse energy effectively drops to zero in null states, but the pulse energy in Figure 3 is often larger than zero even during the apparent “null” states. We therefore suggest that the periodic Q-mode modulation in PSR J1825–0935 is a periodic longitude-stationary intensity modulation occurring in the

¹ <https://data.csiro.au>

² <http://www.atnf.csiro.au/research/pulsar/psrcat/>

³ <https://github.com/weltevrede/psrsalsa>

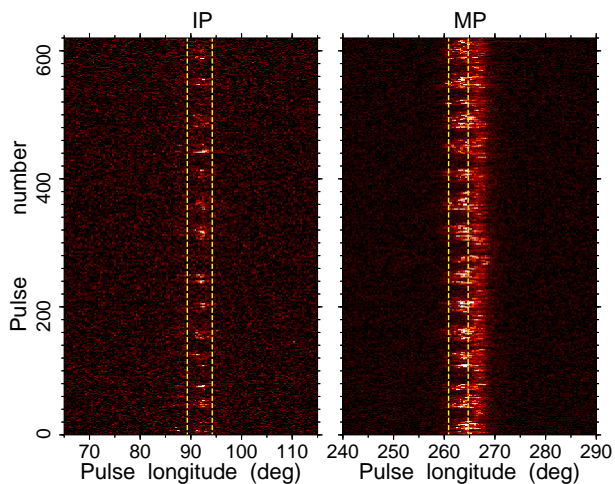


Figure 2. A Q-mode single-pulse stack from the 2014 August 20 observation. The left and right panels show respectively the longitude range around the IP and the MP. The two vertical dashed lines in each panel define a pulse-phase window for computing the pulse energy used in Figure 3. Note that, to see the IP more clearly, the range of the colour scale used in the left panel is different from that in the right panel.

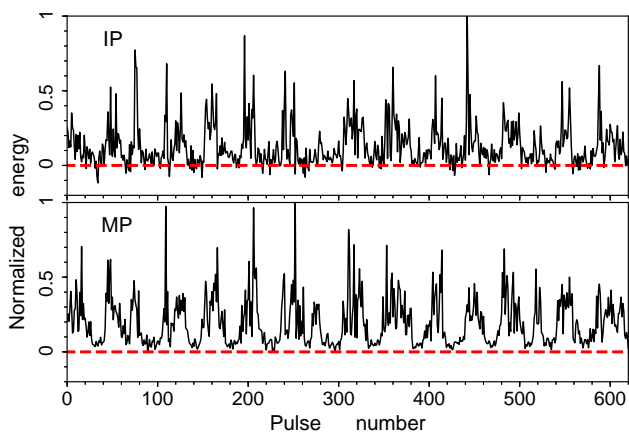


Figure 3. Pulse energy variations for the IP (upper panel) and the leading component of the MP (lower panel) for the 2014 August 20 observation. The pulse phase windows for calculating the pulse energy of each component were defined by the vertical dashed lines in Figure 2.

interpulse and the main pulse rather than periodic pulse nulling. A similar example is PSR B0826–34 whose weak mode had been regarded as a complete null (Biggs et al. 1985). However, a weak emission profile was detected during the “null” states of the pulsar (Esamdin et al. 2005), implying that the “null” state was a weak-emission mode rather than being a null.

3.1 Fluctuation spectra

Figure 2 shows that the modulation period is about $40P_1$, where P_1 is the basic pulse period, approximately 769 ms. Backus et al. (2010) found the Q-mode modulation frequency to be $43P_1$, while Latham et al. (2012) gave a modu-

lation frequency of $46.6P_1$. To investigate the Q-mode modulation frequency further, we carried out an analysis of fluctuation spectra by calculating the longitude-resolved modulation index, the longitude-resolved fluctuation spectrum (LRFS, Backer 1970) and the two-dimensional fluctuation spectrum (2DFS, Edwards & Stappers 2002) for the observations reported here. The longitude-resolved modulation index is a measure of the amount of intensity variability at a given pulse longitude. The LRFS is used to determine the presence of periodicities for each pulse longitude bin. The 2DFS is a different type of fluctuation spectrum that can be used to identify if the emission drifts in pulse longitude from pulse to pulse. Similar to the LRFS, the vertical frequency axis of the 2DFS is expressed as P_1/P_3 , where P_3 corresponds to the $\sim 40P_1$ periodicity of intensity modulation seen in the single-pulse stack. The horizontal frequency axis of the 2DFS is expressed as P_1/P_2 , where P_2 corresponds to the characteristic horizontal time separation between drifting bands. For more details about the analysis, see Weltevrede et al. (2006).

Figure 4 gives an example of our results based on the observation of 2014 August 20. From Figure 4, we can see that the modulation index of the leading component of the MP is higher than that of the trailing component. This is not surprising given the much stronger modulation visible in the leading component of the MP. Examination of the LRFS (Figure 4) shows that, for both the IP and the MP, the spectral peak occurs between 0.0234 and 0.0236 cycles per period (cpp), implying that both the IP and the MP show the same P_3 of $42.6 \pm 0.2 P_1$, consistent with the results of Backus et al. (2010). Fluctuation spectra of the six observations give exactly the same value of P_3 , and therefore we believe that the modulation period for PSR J1825–0935 is quite stable on a timescale of several years. However, the value of P_3 reported by Latham et al. (2012) is somewhat larger than ours, this indicates that there may exist fluctuations in the modulation period on a longer timescale. Furthermore, the 2DFS is perfectly symmetric about the vertical axis for each component. This indicates that subpulses in successive pulses do not drift on average to later or earlier pulse longitudes in either the IP or the MP. There are therefore no drifting subpulses in the Q-mode.

3.2 Phase-locking

A phase-locked relationship between the IP and the MP modulation patterns of PSR J1825–0935 had been found by earlier investigators. Backus et al. (2010) showed that there is a significant correlation between pulse sequences of the $2P_1$ delayed IP and the leading component of the MP. Latham et al. (2012) argued that the IP and the MP pulse sequences are offset in modulation phase by approximately 12 rotation periods. We investigated if there are any phase relations between the $42.6P_1$ modulation patterns observed in the IP and the MP by correlating the measured pulse energies for successive pulses in the IP and the MP of the observation of 2014 August 20. The cross-correlation function (XCF), using the same pulse longitude regions as in Figure 3, is shown in Figure 5. The XCF reaches a maximum value of 0.502 at zero lag, implying that a phase-locked relationship exists between the IP and the following MP. A T-test shows that, at the zero lag, the correlation between

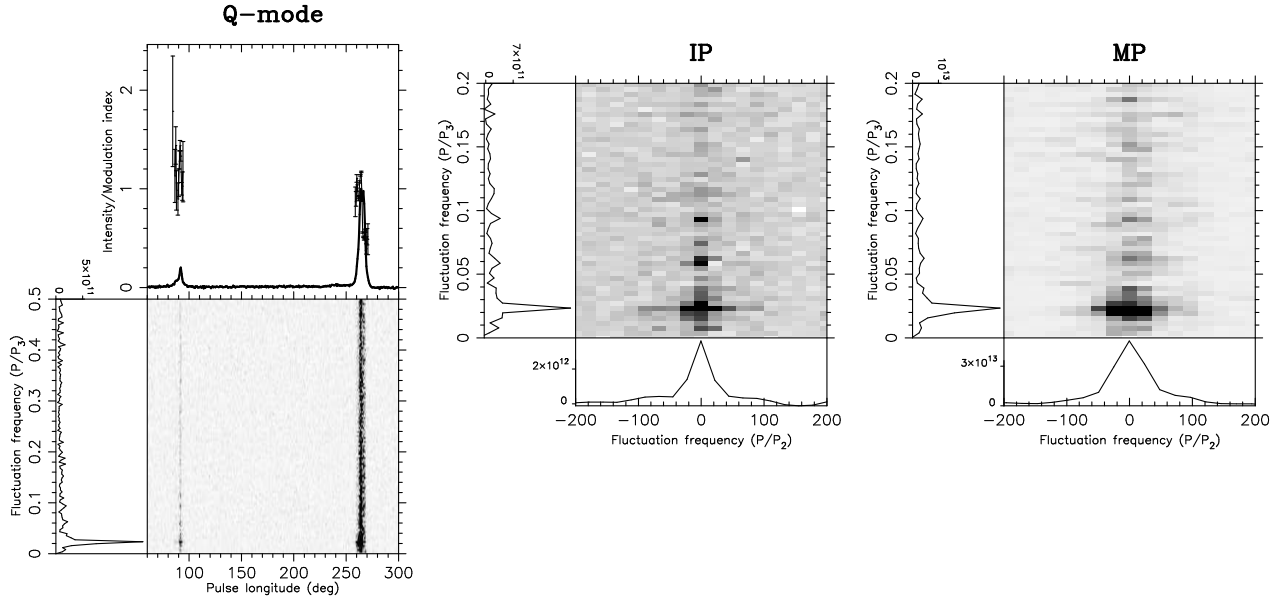


Figure 4. Results of fluctuation analysis for the 2014 August 20 observation. The upper panel of the left column shows the mean pulse profile (solid line) and longitude-resolved modulation index (points with error bars). The LRFs and a side panel showing the horizontally integrated power are given below this panel. The 2DFS and side panels showing horizontally (left) and vertically (bottom) integrated power are plotted for the IP (middle column) and the MP (right column).

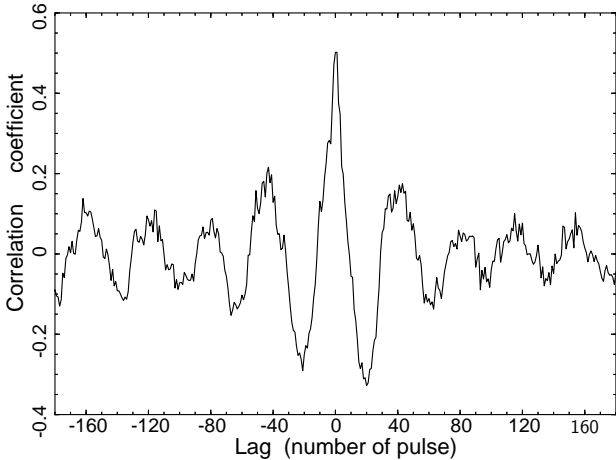


Figure 5. The normalized cross-correlation between the pulse energies of the IP and that of the leading component of the following MP for the 2014 August 20 observation.

the IP intensity and the following MP intensity is significant at 0.01 level. The modulation periodicity is seen in the XCF at delays of about $\pm 40P_1$ and multiples of this. Correlations are smaller than the zero-lag value for all other lags. There is no sign of a significant XCF feature at either $\pm 2P_1$ or $\pm 12P_1$.

3.3 State separation

As a result of the periodic intensity modulation in the Q-mode, the IP and the leading component of the MP switch between a strong state and a weak state periodically (see Figure 3). In this paper, the term “strong state” refers to the strong state of the Q-mode, and the term “weak state” refers

to the weak state of the Q-mode. Identifying the two states is required for further investigation. This is done by comparing the on-pulse energy of the IP of individual pulses with the system noise level. The uncertainty in the on-pulse energy of the IP $\sigma_{\text{IP,on}}$ is given by $\sqrt{N_{\text{on}}}\sigma_{\text{off}}$ (cf. [Bhattacharyya et al. 2010](#)), where N_{on} is the number of on-pulse longitude bins of the IP which was estimated from the mean pulse profile and σ_{off} is the rms of the off-pulse region for single pulses. We classified pulses with on-pulse energy of the IP smaller than $3\sigma_{\text{IP,on}}$ as weak-state pulses and the others as strong-state pulses. Figure 6 shows the results of the state separation for the 2014 August 20 observation. By performing the state separation in this way for six Q-mode observations, we found that 69% of the Q-mode time for PSR J1825–0935 was in the weak state and 31% was in the strong state.

3.4 Polarization

To compare the weak state and the strong state further, we analysed the polarization properties for both states. Of the six observations, only the 2014 April 19 observation has suitable flux and polarization calibration data. Most of the six observations show pure Q-mode emission, however occasional short-duration B-mode emission occurs in the 2014 April 19 observation. To investigate the polarization properties of the weak and strong states, B-mode emission must be removed. As the most remarkable feature of B-mode is the presence of a strong PC component, in order to remove the B-mode pulses from that observation, we calculated the peak signal-to-noise ratio (S/N) for the PC region. That is, the peak S/N is calculated as the ratio between the maximum intensity amplitude of the PC on-pulse region, which was estimated from the B-mode mean pulse profile, in a given rotation period and the standard deviation of the baseline points in the same period ([Yan et al. 2018](#)). Pulses with peak

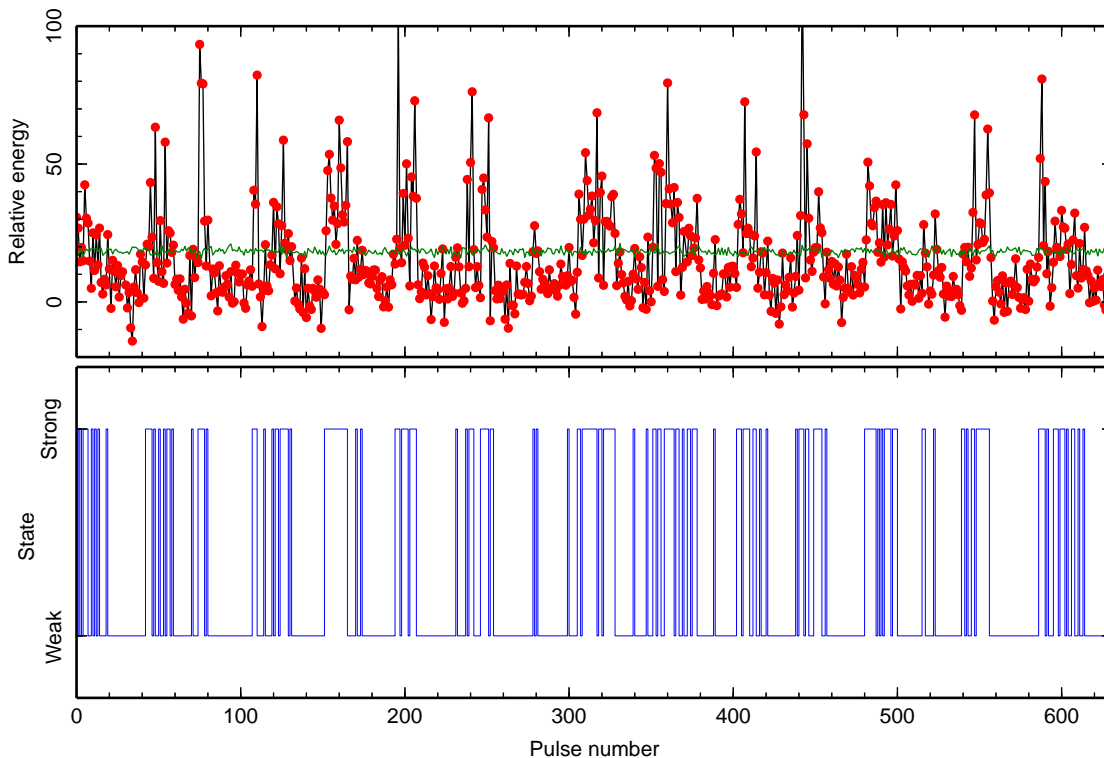


Figure 6. The pulse energy sequence for the IP pulses (upper panel) with their corresponding identified strong/weak state (lower panel) for the 2014 August 20 observation. In the upper panel, a red dot is the on-pulse energy of a given IP pulse and the green line represents the three times level of the rms of the off-pulse region for single pulses. Pulses for which pulse energy below the green line were marked as weak-state pulses and pulses above the green line were marked as strong-state pulses.

S/N larger than 3 were identified as B-mode pulses and then removed from the data. The total number of the resulting Q-mode pulses for the 2014 April 19 observation is 538, which is about 86% of the whole observation.

We show polarization profiles for the 2014 April 19 observation in Figure 7, and Table 1 gives a summary of the polarization parameters for different states. The mean flux density S , the mean linear polarization intensity $\langle L \rangle$, the mean circular polarization intensity $\langle V \rangle$ and the mean absolute circular polarization intensity $\langle |V| \rangle$ were all averaged over the IP/MP on-pulse window. The pulse energy of the IP in the strong state is four times larger than that in the weak state. The MP in the weak state is also relatively weak. The MP has a very strong leading component in the strong state, while the leading component becomes much weaker than the trailing component in the weak state. The fractional linear polarization in the IP of the strong state is higher than that of the weak state, while the fractional circular polarization in the IP of the weak state is a little higher. In the strong state, the circular polarization intensity of the leading component of the MP is stronger than the trailing component. But the circular polarization intensity of the leading component is almost negligible in the weak state. In agreement with Johnston & Kerr (2018), the strong state shows a rapid swing of polarization position angle in its IP.

Figure 7 also shows that, although the trailing edge of the MP of the pulse profile is very similar in the weak and strong states, the polarization of the trailing component of the MP is quite different in the two states. To see the differ-

ence more clearly, we compare total intensity, linearly polarized intensity and circularly polarized intensity of the two states in Figure 8. We can clearly see that both the linear polarization and the circular polarization are relatively stronger in the strong state across the whole MP on-pulse area. This suggests that the trailing component of the MP must also be modulated, that is, the periodic modulation does involve other parts of the magnetosphere, not just the parts where the total intensity is modulated.

4 DISCUSSION AND CONCLUSIONS

The periodic Q-mode modulation of PSR J1825–0935 was discovered more than twenty years ago (Gil et al. 1994), but its nature remains unclear. Latham et al. (2012) related the intensity modulation to drifting subpulses. However, no organized drifting pattern has been observed in observational data. Recently, several periodic non-drift amplitude fluctuation phenomena have been observed in radio pulsar emission. Mitra & Rankin (2017) reported similar longitude-stationary modulation in PSR B1946+35 and they compared modulation in this pulsar with other pulsar modulation phenomena. It was shown that the periodic non-drift amplitude modulation is very different from subpulse drifting and thus was considered to be a new phenomenon. Basu et al. (2016) detected periodic features in 57 pulsars including 29 pulsars that show no systematic drift but periodic amplitude fluctuation. They found a relationship between the drifting phenomenon and the spin-down luminos-

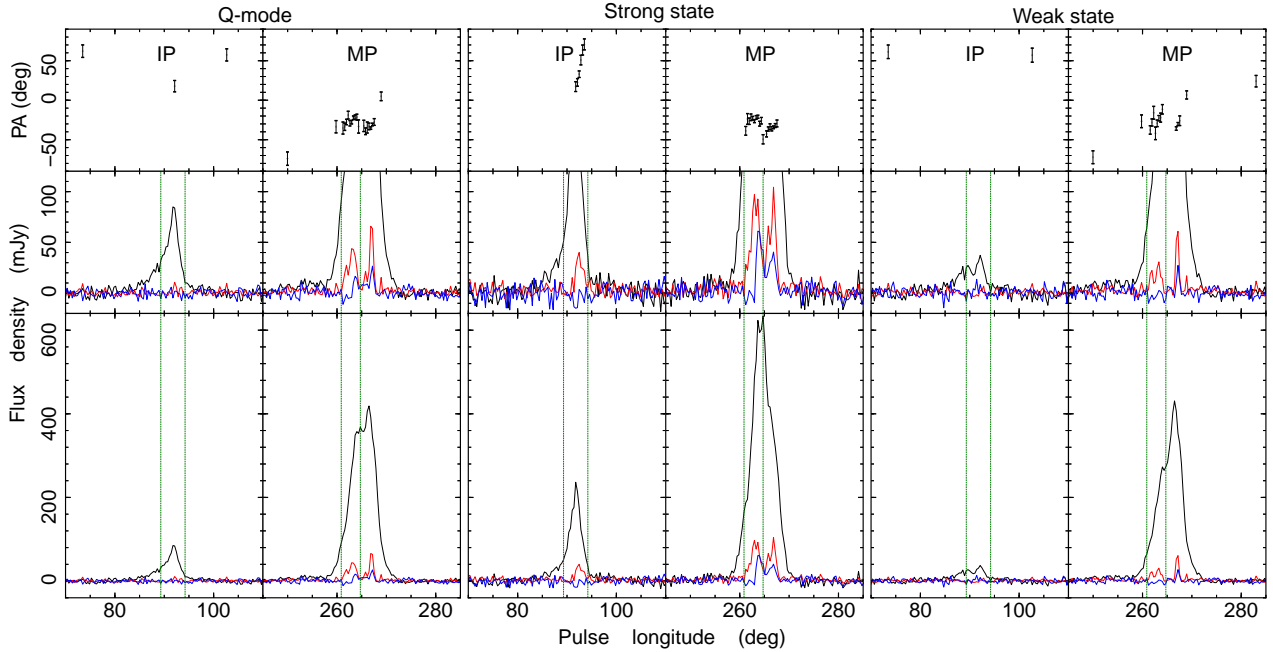


Figure 7. Polarization profiles for the Q-mode pulses (left), the strong-state pulses (middle) and the weak-state pulses (right) for the interpulse and main pulse from the 2014 April 19 observation. The bottom panels show the pulse profiles for total intensity (black line), linearly polarized intensity (red line), and circularly polarized intensity (blue line). The middle panels give expanded plots showing low-level details of the polarization profiles and the top panels give the position angles of the linearly polarized emission. The two vertical dashed lines in each panel define the same pulse-phase window as Figure 2.

Table 1. Flux density and polarization parameters of the IP and the MP for the strong and weak states for the 2014 April 19 observation.

State	IP					MP				
	S (mJy)	W_{50} ($^{\circ}$)	$\langle L \rangle / S$ (%)	$\langle V \rangle / S$ (%)	$\langle V \rangle / S$ (%)	S (mJy)	W_{50} ($^{\circ}$)	$\langle L \rangle / S$ (%)	$\langle V \rangle / S$ (%)	$\langle V \rangle / S$ (%)
Q-mode	29.4	2.9	2.3	-2.7	11.4	163.9	5.7	7.7	1.5	3.3
Strong state	67.2	2.5	12.6	-3.1	9.3	218.6	5.0	12.8	4.9	6.1
Weak state	15.8	5.3	4.1	3.6	23.8	144.4	4.9	6.0	0.2	3.3

ity \dot{E} . In those 57 pulsars, pulsars showing subpulse drifting are seen to lie below $\dot{E} \simeq 2 \times 10^{32} \text{ erg s}^{-1}$, whereas other pulsars with \dot{E} above this value all showed non-drift amplitude modulation. PSR J1825–0935 has an $\dot{E} \sim 4.6 \times 10^{33} \text{ erg s}^{-1}$ (Yuan et al. 2010), and thus lies in the non-drift amplitude modulation group.

Another similar phenomenon is periodic nulling that has been widely reported in many pulsars (Herfindal & Rankin 2007, 2009; Rankin & Wright 2008; Rankin et al. 2013; Gajjar et al. 2014, 2017; Basu et al. 2017). The periodicities of the amplitude modulation are very similar to periodic nulling, causing Basu et al. (2017) to propose that they both may have a common origin. Herfindal & Rankin (2007) used the rotating subbeam carousel model to account for periodic nulling, in which the conal subbeams rotate around the central core component. When the line of sight passes through the empty region between two conal subbeams or through an extinguished subbeam, nulling occurs, and this can repeat after certain spin periods of the pulsar. However, Basu et al. (2017) found that the missing line of sight model

did not adequately explain the periodic nulling observed in many pulsars, particularly in pulsars with core components. Additionally, because of lack of phase memory and partial nulls, the missing line of sight model is probably not applicable to the quasi-periodic feature seen in PSR J1741–0840 (Gajjar et al. 2017). For the periodic Q-mode modulation of PSR J1825–0935 reported in this paper, the IP and the MP switch between a strong state and a weak state periodically. The weak state shows relatively weak emission in the IP and the leading component of the MP, but not complete nulls. This does not fit very well with the missing line of sight model. Furthermore, as is shown in Figure 8, the trailing edge of the MP of the pulse profile is similar in the weak and strong states, but the polarization of the trailing component of the MP differs significantly in the two states. The polarization difference is not readily explained with the rotating subbeam carousel model.

Our results show that the periodic Q-mode modulation of PSR J1825–0935 is caused by regular switching between two emission states. It is possible that the periodic modu-

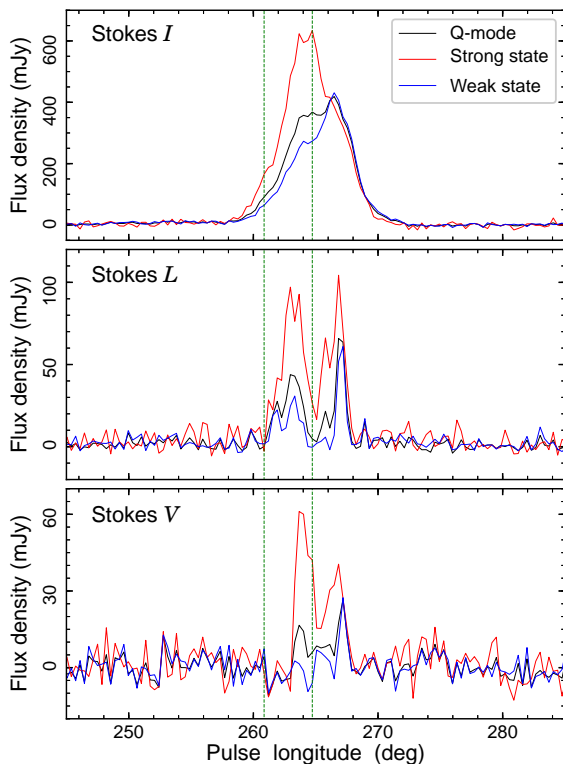


Figure 8. The comparison of the polarization properties of the MP in the strong state and the weak state. The top, middle and bottom panels show respectively the total intensity, linearly polarized intensity and circularly polarized intensity for different states. The two vertical dashed lines in each panel define the same pulse-phase window as the right panel of Figure 2.

lation is actually a mode change. However, in most pulsars, mode changing is not periodic and so the relationship between these two phenomena is somewhat unclear. Nevertheless, we argue that the periodic modulations in the Q-mode of PSR J1825–0935 result from similarly periodic fluctuations in the magnetospheric field currents that are not directly related to sub-pulse drifting.

In agreement with earlier results, we show that there is a phase-locked relationship between the IP and MP modulations in the Q-mode of PSR J1825–0935. Similar phase-locked features were also detected in PSRs B1702–19 (Weltevrede et al. 2007) and B1055–52 (Weltevrede et al. 2012). No phase lag in the modulation patterns was found in our data, implying that the IP and the following MP have correlated intensity variations. The zero-lag phase-locked feature is found to be identical in all six observations we used. This implies the phase-locked feature is sustained over several years and probably a permanent feature of PSR J1825–0935.

Recently, a close correlation between the emission variability and the rotational properties has been reported in a number of pulsars (Kramer et al. 2006; Lyne et al. 2010; Keith et al. 2013; Brook et al. 2014, 2016; Kou et al. 2018). These pulsars provide direct observational evidence for the connection between magnetosphere behaviour and rotational behaviour. For PSR J1825–0935, the variation of the ratio of the amplitudes of the PC and MP (which indi-

cates the Q-mode or B-mode) has been found to correlate with the variation of spin-down rate in a long timescale (~ 10 yr) (Lyne et al. 2010). It is possible to determine the spin-down rates in the weak and strong states of the Q-mode separately by using standard pulsar timing techniques on each state. However, more single-pulse pure Q-mode observational data spanning a long timescale are required for this study.

PSR J1825–0935 is commonly considered to be an orthogonal rotator where the IP and MP are emitted from two opposite magnetic poles. In a recent work, Johnston & Kerr (2018) presented a high quality polarization profile for PSR J1825–0935. A rapid swing of polarization position angle is seen in both the main pulse and the interpulse providing new evidence for the two-pole model. In the two-pole geometry, the same modulation in the IP and MP of PSR J1825–0935 is puzzling, because it requires information transfer between the two opposite magnetic poles. Some investigators have suggested the possibility of global change in the pulsar magnetosphere on very short timescales (Latham et al. 2012). Another possible explanation is that the two magnetic poles are affected simultaneously through non-radial oscillations of the body of the neutron star itself (Weltevrede et al. 2007). At present, neither of these explanations is very compelling and maybe the one-pole model of Dyks et al. (2005) should be further considered. It is clear that more investigation of possible emission models is needed to clarify the mechanism(s) responsible for the observed phenomena.

ACKNOWLEDGEMENTS

This work is supported by National Basic Research Program of China (973 Program 2015CB857100), National Natural Science Foundation of China (Nos. U1831102, U1731238, U1631106, 11873080, U1838109), the Strategic Priority Research Program of Chinese Academy of Sciences (No. XDB23010200), the National Key Research and Development Program of China (No. 2016YFA0400800), the 2016 Project of Xinjiang Uygur Autonomous Region of China for Flexibly Fetching in Upscale Talents and the CAS “Light of West China” Program (2016-QNXZ-B-24 and 2017-XBQNXZ-B-022). The Parkes radio telescope is part of the Australia Telescope, which is funded by the Commonwealth of Australia for operation as a National Facility managed by the Commonwealth Scientific and Industrial Research Organisation.

REFERENCES

- Backer D. C., 1970, *Nature*, 227, 692
- Backus I., Mitra D., Rankin J. M., 2010, *MNRAS*, 404, 30
- Basu R., Mitra D., Melikidze G. I., Maciesiak K., Skrzypczak A., Szary A., 2016, *ApJ*, 833, 29
- Basu R., Mitra D., Melikidze G. I., 2017, *ApJ*, 846, 109
- Bhattacharyya B., Gupta Y., Gil J., 2010, *MNRAS*, 408, 407
- Biggs J. D., McCulloch P. M., Hamilton P. A., Manchester R. N., Lyne A. G., 1985, *MNRAS*, 215, 281
- Brook P. R., Karastergiou A., Buchner S., Roberts S. J., Keith M. J., Johnston S., Shannon R. M., 2014, *ApJ*, 780, L31
- Brook P. R., Karastergiou A., Johnston S., Kerr M., Shannon R. M., Roberts S. J., 2016, *MNRAS*, 456, 1374

- Dyks J., Zhang B., Gil J., 2005, *ApJ*, 626, L45
- Edwards R. T., Stappers B. W., 2002, *A&A*, 393, 733
- Esamdin A., Lyne A. G., Graham-Smith F., Kramer M., Manchester R. N., Wu X., 2005, *MNRAS*, 356, 59
- Fowler L. A., Wright G. A. E., 1982, *A&A*, 109, 279
- Fowler L. A., Wright G. A. E., Morris D., 1981, *A&A*, 93, 54
- Gajjar V., Joshi B. C., Wright G., 2014, *MNRAS*, 439, 221
- Gajjar V., Yuan J. P., Yuen R., Wen Z. G., Liu Z. Y., Wang N., 2017, *ApJ*, 850, 173
- Gil J. A., et al., 1994, *A&A*, 282, 45
- Herfindal J. L., Rankin J. M., 2007, *MNRAS*, 380, 430
- Herfindal J. L., Rankin J. M., 2009, *MNRAS*, 393, 1391
- Hermesen W., et al., 2017, *MNRAS*, 466, 1688
- Hobbs G., et al., 2011, *PASA*, 28, 202
- Hotan A. W., van Straten W., Manchester R. N., 2004, *PASA*, 21, 302
- Johnston S., Kerr M., 2018, *MNRAS*, 474, 4629
- Keith M. J., Shannon R. M., Johnston S., 2013, *MNRAS*, 432, 3080
- Kou F. F., Yuan J. P., Wang N., Yan W. M., Dang S. J., 2018, *MNRAS*, 478, L24
- Kramer M., Lyne A. G., O'Brien J. T., Jordan C. A., Lorimer D. R., 2006, *Science*, 312, 549
- Latham C., Mitra D., Rankin J., 2012, *MNRAS*, 427, 180
- Lyne A., Hobbs G., Kramer M., Stairs I., Stappers B., 2010, *Science*, 329, 408
- Maciesiak K., Gil J., Ribeiro V. A. R. M., 2011, *MNRAS*, 414, 1314
- Manchester R. N., et al., 2001, *MNRAS*, 328, 17
- Manchester R. N., Hobbs G. B., Teoh A., Hobbs M., 2005, *AJ*, 129, 1993
- Manchester R. N., et al., 2013, *PASA*, 30, e017
- Mitra D., Rankin J., 2017, *MNRAS*, 468, 4601
- Morris D., Graham D. A., Bartel N., 1981, *MNRAS*, 194, 7P
- Rankin J. M., Wright G. A. E., 2008, *MNRAS*, 385, 1923
- Rankin J. M., Wright G. A. E., Brown A. M., 2013, *MNRAS*, 433, 445
- Staveley-Smith L., et al., 1996, *PASA*, 13, 243
- van Straten W., Bailes M., 2011, *PASA*, 28, 1
- van Straten W., Manchester R. N., Johnston S., Reynolds J. E., 2010, *PASA*, 27, 104
- Wang N., Manchester R. N., Johnston S., 2007, *MNRAS*, 377, 1383
- Weltevrede P., 2016, *A&A*, 590, A109
- Weltevrede P., Edwards R. T., Stappers B. W., 2006, *A&A*, 445, 243
- Weltevrede P., Wright G. A. E., Stappers B. W., 2007, *A&A*, 467, 1163
- Weltevrede P., Wright G., Johnston S., 2012, *MNRAS*, 424, 843
- Yan W. M., et al., 2011, *MNRAS*, 414, 2087
- Yan W. M., Wang N., Manchester R. N., Wen Z. G., Yuan J. P., 2018, *MNRAS*, 476, 3677
- Yuan J. P., Wang N., Manchester R. N., Liu Z. Y., 2010, *MNRAS*, 404, 289

This paper has been typeset from a $\text{\TeX}/\text{\LaTeX}$ file prepared by the author.